COMPOSITE RUDDER SKIN OPTIMIZATION WITH TAILORED THERMAL RESIDUAL STRESSES

Mattos, Cristiano Tavares de, ct.mattos@uol.com.br
Hernandes, José Antônio, hernandes@ita.br
Instituto Tecnológico de Aeronáutica

Abstract. *The main scope of this work is to develop an efficient optimization procedure using the MSC.NASTRAN (Solution 200) in order to evaluate complex structures made of composite material taking advantage of the thermal residual stresses into elastic buckling problems. Thermal residual stresses introduced during the manufacturing process can be tailored to significantly increase the buckling loads of the composite structures, therefore the optimization procedure, herein proposed, improves the design of the structure taking the induced thermal state into account. The optimization procedure requires the analyses of thermal and buckling problems for complex structures, thus the use of finite element method is also required. The analysis study used to validate the proposed procedure, consists in the design optimization of an aeronautic rudder skin.*

Keywords*: optimization, composite, thermal residual stresses, NASTRAN, buckling*

1. INTRODUCTION

The thermal residual stresses introduced during the manufacturing process of composite structures are seldom, or usually not taken into account during the design and analysis of complex structures. The presence of such manufacturing stresses may significantly affect the structural stability response.

The idea for using the TRS (thermal residual stresses) was introduced by Almeida and Hansen (1997), they have shown that its possible to enhance the elastic buckling loads of composite plates by tailoring the TRS, their results were confirmed by Sarah Babu and Kant (1998). Later the idea of using optimization techniques in order to determine optimal designs that take full advantage of the presence of TRS was developed for plates with stiffeners by Andrade (2002). Seeing that nowadays, the use of composite materials had became a trend into aerospace structures, the need for an optimization technique for complex structures taking the TRS into account is necessary, therefore it is proposed a procedure that uses the optimization solution from the commercial software (MSC.NASTRAN SOL200) in order to efficiently assist the engineer on its work.

The analysis studies used to validate the procedure consist in the design optimization of an aeronautical rudder skin. The rudder is manufactured by one-shot process, where the entire structure is cured into an autoclave and no sub-assemblies are needed. Four analyses are performed with different temperature conditions and the results are commented.

2. STRUCTURAL OPTIMIZATION

2.1. Stability problem formulation

The problem under consideration has three main pieces. The first piece is the calculation of the thermally induced effects due to the cure/consolidation, the second is the calculation of the structure prebuckling state and the final is the buckling calculation. The eigenvalue problem to be solved is

$$\left(\left[K\right]+\left[K_G^R\right]-\lambda\left[K_G^0\right]\right)\left\{\delta\right\}=\left\{0\right\} \tag{1}$$

Respectively, K, K_G^R, K_G^0 are, the stiffness matrix, the thermal geometric stiffness matrix, and the prebuckling geometric stiffness matrix. The least eigenvalue λ corresponds to the buckling load of the structure for the vector of unknown nodal displacements, $\{\delta\}$.

The solution procedure for the structural stability problem in Eq. (1) using the finite element method includes the following steps:

1. calculation of stiffness matrix for the structure, K;
2. solution of the thermoelastic problem by linear analysis to obtain the TRS and subsequently the computation of the thermal geometric stiffness matrix, K_G^R;
3. solution of the prebuckling problem to compute the stress resultants due to prebuckling load, followed by the computation of the prebuckling geometric stiffness matrix, K_G^0;

4. solution of the eigenvalue problem Eq. (1).

2.2. Optimization method

The optimization procedure herein described uses two of the MSC. NASTRAN solutions, the linear buckling and the optimization solutions, called respectively SOL105 and SOL200. The first one solves the buckling problem described by Eq. (1), including the pre-thermal load, and the second one optimizes the structure by defined design variables and constraints.

The SOL200 does not recognize the matrix, K_G^R , which comes from the pre-thermal loading condition so the eigenvalue problem from Eq. (1) cannot be used as a constraint. Therefore, reorganizing the Eq. (1) forcing the thermal geometric stiffness matrix to be multiplied by λ ,

$$\left(\left[K\right]-\lambda\left(\left[K_G^0\right]-\beta\left[\bar{k}_G^R\right]\right)\right)\left\{\delta\right\}=\left\{0\right\} \tag{2}$$

In Eq.(2), $\beta=\Delta T/\lambda$ is defined as thermal correction factor loading, and $\left[\bar{k}_G^R\right]$ is the thermal geometric stiffness matrix for a unit temperature variation $\left(\Delta T=1\right)$.

The eigenvalue solution for the Eq. (2) is simple since both loads (thermal and mechanical) are applied simultaneously, requiring only one linear static solution to compute the stress resultants for evaluating the geometric stiffness matrix. Eq. (2) can be used as a constraint into SOL200 and gives the same eigenvalue results as Eq. (1) when the structural boundary conditions are identical for both loading conditions.

The workflow in Fig. 1 shows the proposed optimization procedure.

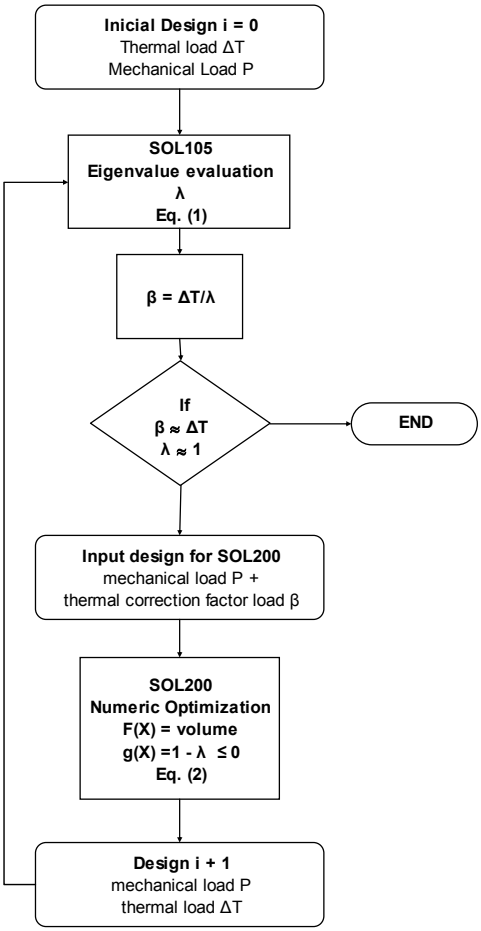

Figure 1 Optimization procedure workflow

In summary, the procedure follows two steps until the analysis reaches its convergence. As first step the eingenvalue λ is evaluated using the SOL105 applying the pre-thermal loading, ΔT , and mechanical loading, P separately. After,

as second step, the optimization solution (SOL200) is run using β as the temperature loading at the same time as the mechanical load, P .

The procedure above shall be used with caution since by Eq. (2) it can be noted that multiplies both, thermal and mechanical geometric stiffness matrix. This situation obliges the boundary condition to be the same for both thermal and mechanical loads. Since in real life the previous condition is not possible, seeing that during the cure/consolidation processes the structure is usually unconstrained, the suggestion here is to optimize regions where the boundary influence is negligible. Therefore the region of optimization shall be carefully studied and previous analysis shall be made in order to check such influence.

2.2. Case Studies

The geometry, loads and finite element mesh of the rudder was obtained from Riscado (2004) and used to evaluate the proposed optimization methodology. Material, boundary condition and also the structural stacking sequence were modified for the optimization where the Fig. 2 a) shows the rudder skin mesh and b) the spars, ribs and hinge points.

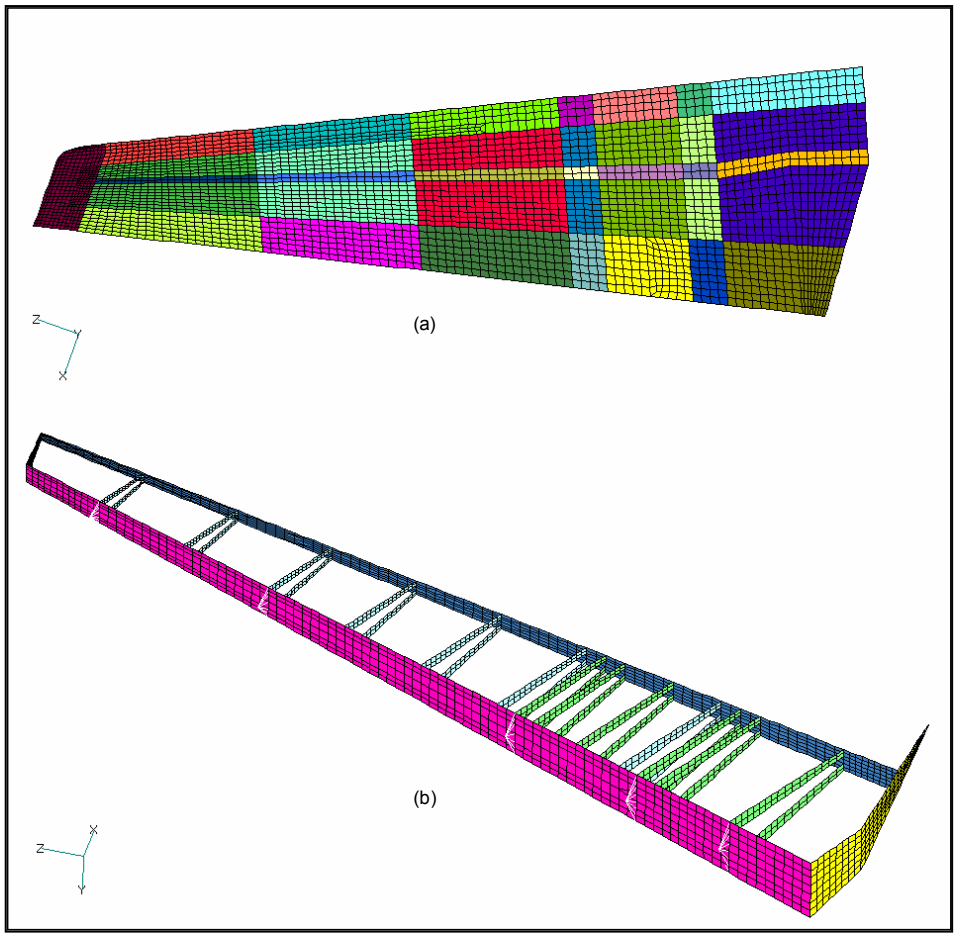

Figure 2 Rudder Finite Element Model
(a) rudder skin mesh
(b) spars, ribs and hinge points

The rudder skin was divided into panels with different laminate lay-up, Fig. 3 shows the different regions where Tab. 1 indicates its staking sequence. The rudder skin has the same properties at both sides since the load conditions are symmetrical. The adjacent structures like spars and ribs are not within the scope of this optimization, and Tab. 2 shows their unmodified properties. The material angle is defined along the front spar axis.

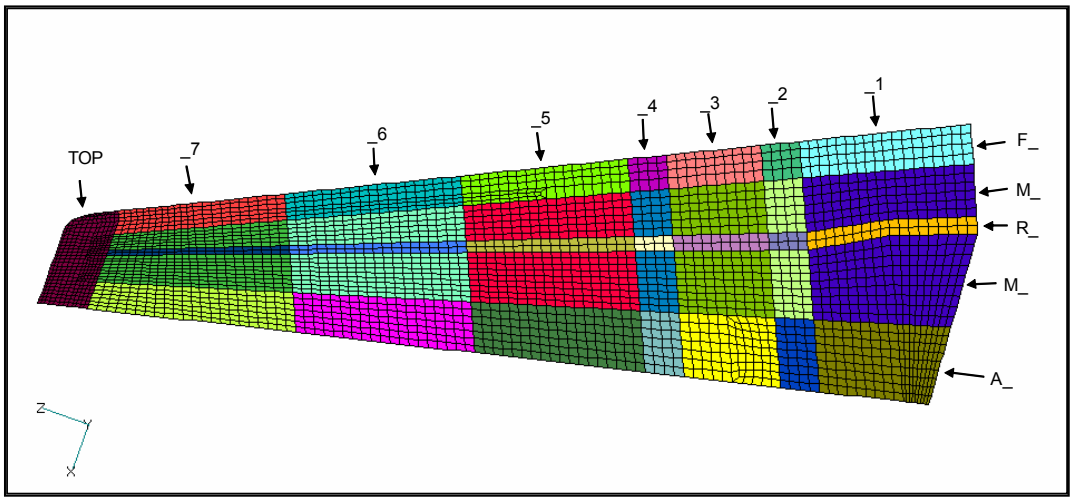

Figure 3 Rudder skin optimization panels

Table 1 Rudder skin staking/material properties

Panel	Material	Stacking Orientation	Panel	Material	Stacking Orientation
TOP	Tape	(0,90,45,-45,-45,45,90,0)s	A4	Tape	(0,90,45,-45,-45,45,90,0)s
F7	Tape	(0,90,45,-45,-45,45,90,0)s	R4	Tape	$[(0,90)_5$,45,-45,-45,45,90,0]s
M7	Tape	(0,90,45,-45,-45,45,90,0)s	F3	Tape	(0,90,45,-45,-45,45,90,0)s
A7	Tape	(0,90,45,-45,-45,45,90,0)s	M3	Tape	(0,90,45,-45,-45,45,90,0)s
R7	Tape	$[(0,90)_3$,45,-45,-45,45,90,0]s	A3	Tape	(0,90,45,-45,-45,45,90,0)s
F6	Tape	(0,90,45,-45,-45,45,90,0)s	R3	Tape	$[(0,90)_5$,45,-45,-45,45,90,0]s
M6	Tape	(0,90,45,-45,-45,45,90,0)s	F2	Tape	(0,90,45,-45,-45,45,90,0)s
A6	Tape	(0,90,45,-45,-45,45,90,0)s	M2	Tape	(0,90,45,-45,-45,45,90,0)s
R6	Tape	$[(0,90)_3$,45,-45,-45,45,90,0]s	A2	Tape	(0,90,45,-45,-45,45,90,0)s
F5	Tape	(0,90,45,-45,-45,45,90,0)s	R2	Tape	$[(0,90)_5$,45,-45,-45,45,90,0]s
M5	Tape	$[(0,90)_3$,45,-45,-45,45,90,0]s	F1	Tape	(0,90,45,-45,-45,45,90,0)s
A5	Tape	(0,90,45,-45,-45,45,90,0)s	M1	Tape	(0,90,45,-45,-45,45,90,0)s
R5	Tape	$[(0,90)_4$,45,-45,-45,45,90,0]s	A1	Tape	(0,90,45,-45,-45,45,90,0)s
F4	Tape	(0,90,45,-45,-45,45,90,0)s	R1	Tape	$[(0,90)_5$,45,-45,-45,45,90,0]s
M4	Tape	(0,90,45,-45,-45,45,90,0)s			

Table 2 Rudder spars and rib skin staking/material properties

Structural Region	Material	Staking Orientation
Front Spar	Fabric	$[(0,45)_3$,0]s
Rear Spar	Fabric	[(0,45)2]s
Ribs 0 and 14	Fabric	$[(45,90)_2$,45]s
Ribs 1,2,3,5,6 and 7	Fabric	(90,45,45,90,45,90,45,45,90)
Ribs 4,8 a 13	Fabric	$[(90,45)_2$,90]s

The ribs are sequenced numbered from bottom to top as the panels.

The referenced mechanical properties for fabric and tape carbon/epoxy are presented into Tab. 3.

Table 3 Material mechanical properties

	E_1 (MPa)	E_2 (MPa)	ν_{12}	G_{12} (MPa)	G_{13} (MPa)	G_{23} (MPa)	α_1 (1/°C)	α_2 (1/°C)
Fabric	59950	57100	0.056	3710	3710	3710	-	-
Tape	154500	11130	0.304	6980	6980	3360	-0.17×10^{-6}	23.1×10^{-6}

The critical aerodynamic load for the rudder structure was defined by Riscado (2004) and denominated hardover, its pressure distribution along the rudder skin chord is shown at Fig. 4. The x axis at Fig. 4 is normalized by the rudder chord wise from the leading to trailing edge along the rudder span wise. The positive values at Fig 4 correspond to compression and negative to suction.

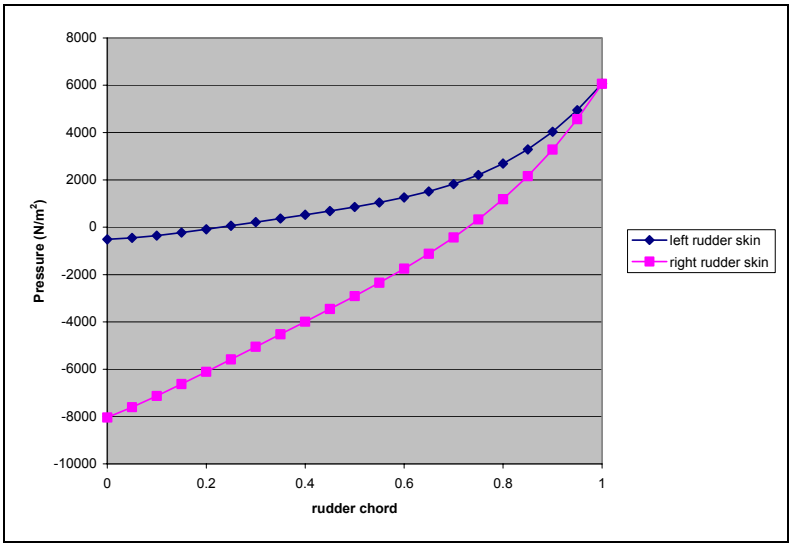

Figure 4 Rudder skin critical load, hardover

The boundary conditions for the rudder structure are marked in Fig. 5. There are five hinge fittings along the spar modeled by rigid elements linked to the constrained nodes simulating the operational boundary condition.

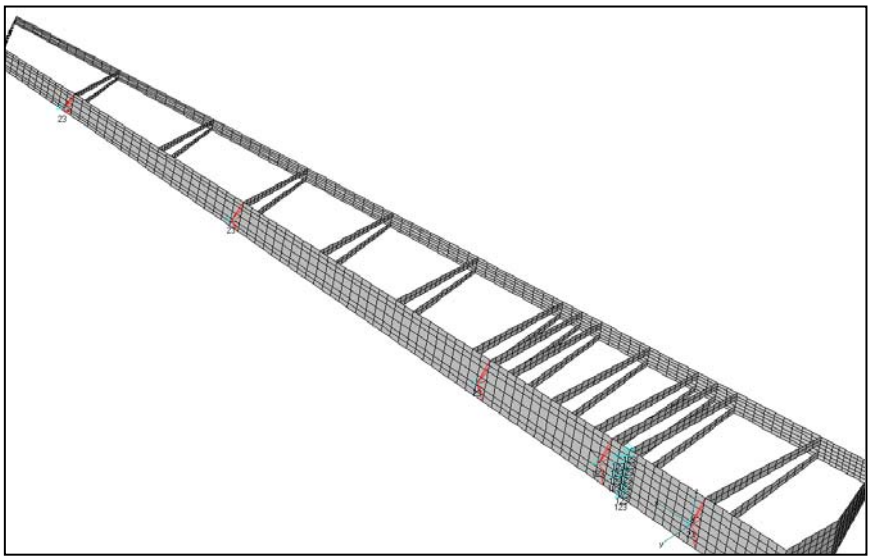

Figure 5 Boundary conditions and restraints

Table 4 shows the case studies and the differential temperature loads applied for each optimization. The optimization procedure from Fig. 1 was used for three different differential temperatures, and for comparison the model was also optimized using SOL200 without the temperature loading (case 1).

Table 4 Material mechanical properties

Case Study	Operational Temperature (°Celsius) T_O	Condition	Cure Temperature (°Celsius) T_C	Diferential Temperature ($\Delta T = T_O - T_C$)-
1	-	-	-	0
2	+23	Ambient	180	-157
3	+82	High	180	-98
4	-55	Low	180	-235

The design variables (DV) consist of each ply thickness of the rudder skin, which can vary continuously (not discrete) during the optimization. The procedure above will handle with 282 DV for each case study, the amount of DV came from the number of panels and plies specified in Tab. 1. The initial thicknesses for all DV were 0.15 mm, though during the optimization it can vary from 0.01 (lower bound) up to 0.30 (upper bound) mm, these limitations are called the side constraints.

The objective function, F(x), to be minimized for all case studies is the rudder weight, calculated automatically during the optimization at SOL200.

The only inequality constraint in the problem requires the first eigenvalue λ_1 to be higher than one, meaning that the applied load is smaller than the buckling load:

$$g(\vec{x}) = 1 - \lambda_1 \leq 0 \tag{3}$$

Although we have already defined the side limits for the DV it is important to notice that internally to SOL200 the concept of movable limits is also used by defining the variable DELX which is the ratio of change allowed for the DV during each interaction between the DOT optimizer and the approximated model. As an important remark the DELX parameter shall be monitored during the optimization procedure, since a premature convergence may happen in case DELX is too small or even divergence for a too big DELX. It is important to try many values of DELX when using SOL200 in order to find an adequate value for a good optimization convergence.

During all optimization steps of SOL200, the constraint Eq. (3) is evaluated not only for the fundamental but also for the first 20 eigenvalues of the structure. This is necessary in order to avoid convergence difficulties during the optimization iterations caused by the change of the fundamental mode shape.

3. RESULTS

Tables 5 thru 8 show the summary of the results obtained using the proposed procedure for optimizing the rudder structure at different ΔT . Each row (step) of the Tab. 5-8 represents one loop of optimization according to Fig. 1, resulting in a new Design (i+1), obtained after a run of SOL 200.

Table 5 Summary for ΔT=0

	Inicial Parameters		**Results**				**Delta % F(X)**	
step	**β**	**DELX**	**g(X)**	**F(X)**	**λ1**	**iterations SOL 200**	**ΔF(X)%**	**ΔF(X)% acum**
0	-	-	-	57314130	1.446	-	-	-
1	-	50%	3.032E-03	41995200	0.997	28	-26.73%	-26.73%

Table 6 Summary for ΔT=-98 °C

	Inicial Parameters		Results				Delta % F(X)	
step	β	DELX	g(X)	F(X)	λ1	iterations SOL 200	ΔF(X)%	ΔF(X)% accum
0	-	-	-	57314130	1.753	-	-	-
1	-55.89	30%	3.666E-04	42213370	1.037	8	-26.35%	-26.35%
2	-94.54	50%	7.897E-04	41689320	1.004	9	-1.24%	-27.26%
3	-97.58	100%	4.501E-04	41673440	1.000	1	-0.04%	-27.29%

Table 7 Summary for ΔT=-157 °C

	Inicial Parameters		Results				Delta % F(X)	
step	β	DELX	g(X)	F(X)	λ1	iterations SOL 200	ΔF(X)%	ΔF(X)% accum
0	-	-	-	57314130	1.898	-	-	-
1	-82.71	50%	1.044E-03	40029420	0.832	25	-30.16%	-30.16%
2	-188.78	30%	1.100E-03	38528490	0.917	23	-3.75%	-32.78%
3	-171.26	50%	1.100E-03	38146970	0.969	33	-0.99%	-33.44%
4	-161.96	50%	5.229E-04	37889630	0.995	25	-0.67%	-33.89%
5	-157.86	100%	4.531E-04	37846840	0.999	6	-0.11%	-33.97%

Table 8 Summary for ΔT=-235 °C

	Inicial Parameters		Results				Delta % F(X)	
step	β	DELX	g(X)	F(X)	λ1	iterations SOL 200s	ΔF(X)%	ΔF(X)% accum
0	-	-	-	57314130	1.950	-	-	-
1	-120.49	30%	4.246E-04	39749790	0.948	24	-30.65%	-30.65%
2	-247.98	100%	-5.225E-04	39503480	0.999	11	-0.62%	-31.08%

The last column of Tables 5 to 8 present the percentage weight reduction obtained for the optimization in each temperature. These results are illustrated in Fig.6. It can be noticed that the best weight reduction occurred with the ambient temperature ($\Delta T = -157$).

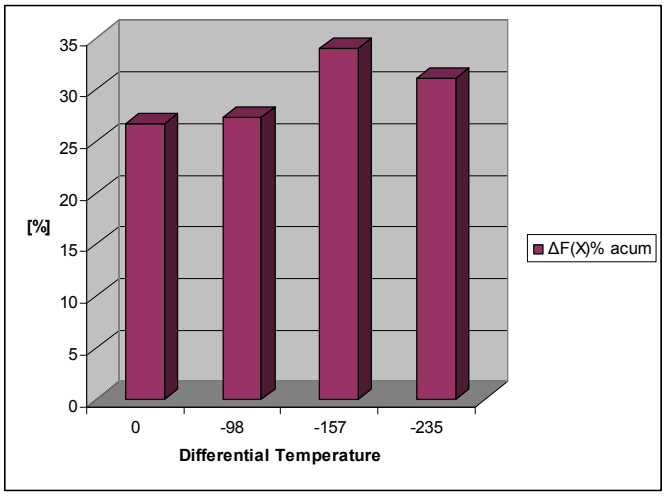

Figure 6 Percentage of weight reduction

Figures 7 thru 10 show the final thickness of the rudder skin obtained for each temperature after optimization for the regions defined according to Tab. 1

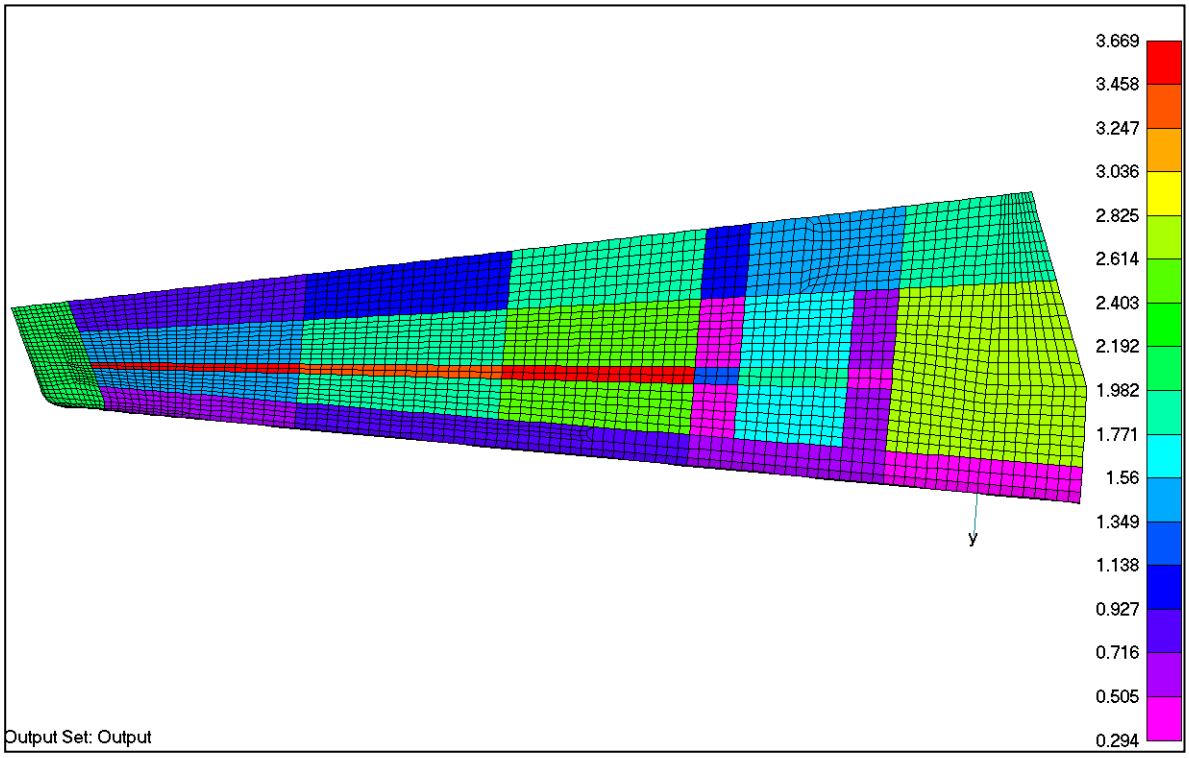

Figure 7 Rudder skin thickness for ΔT=0

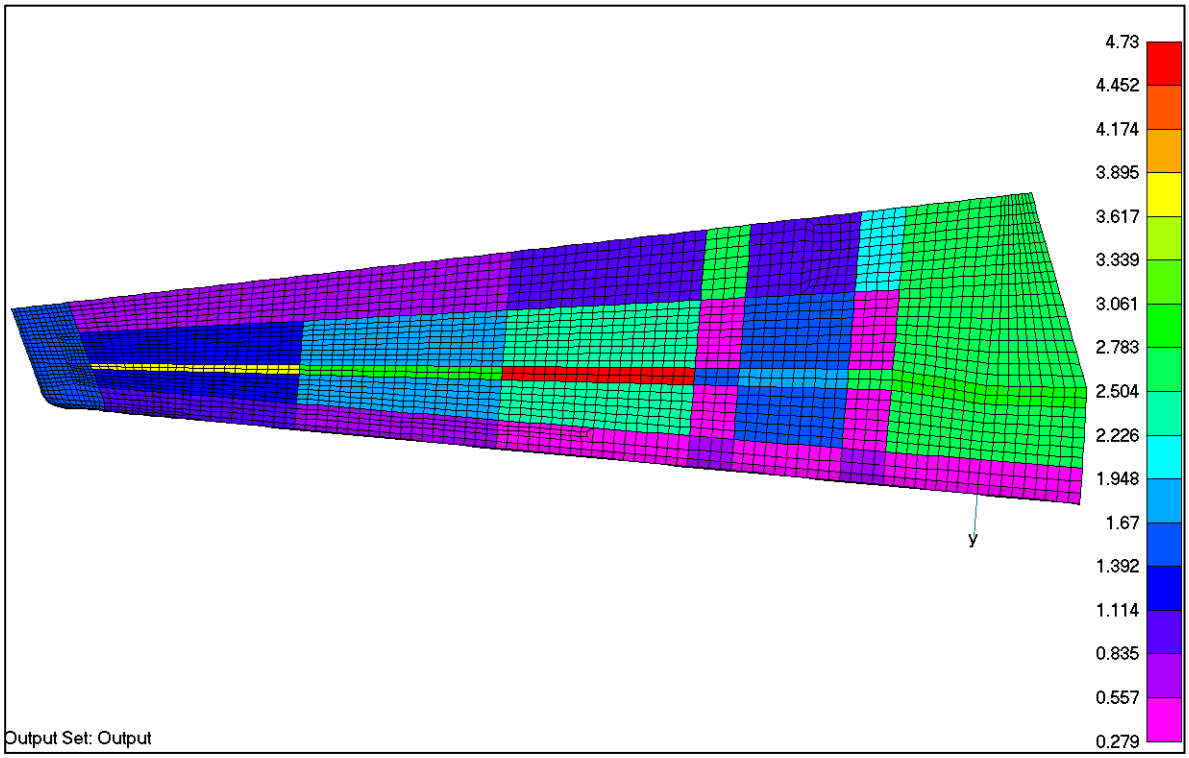

Figure 8 Rudder skin thickness for ΔT=-98

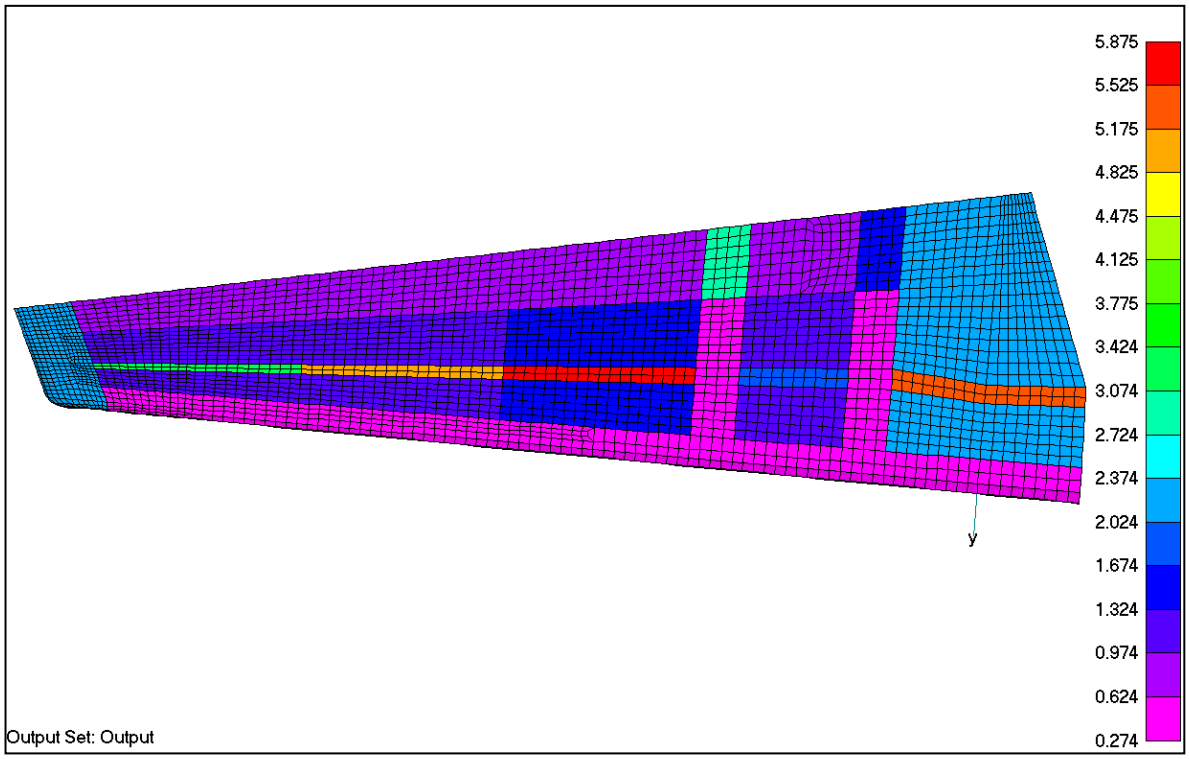

Figure 9 Rudder skin thickness for ΔT=-157

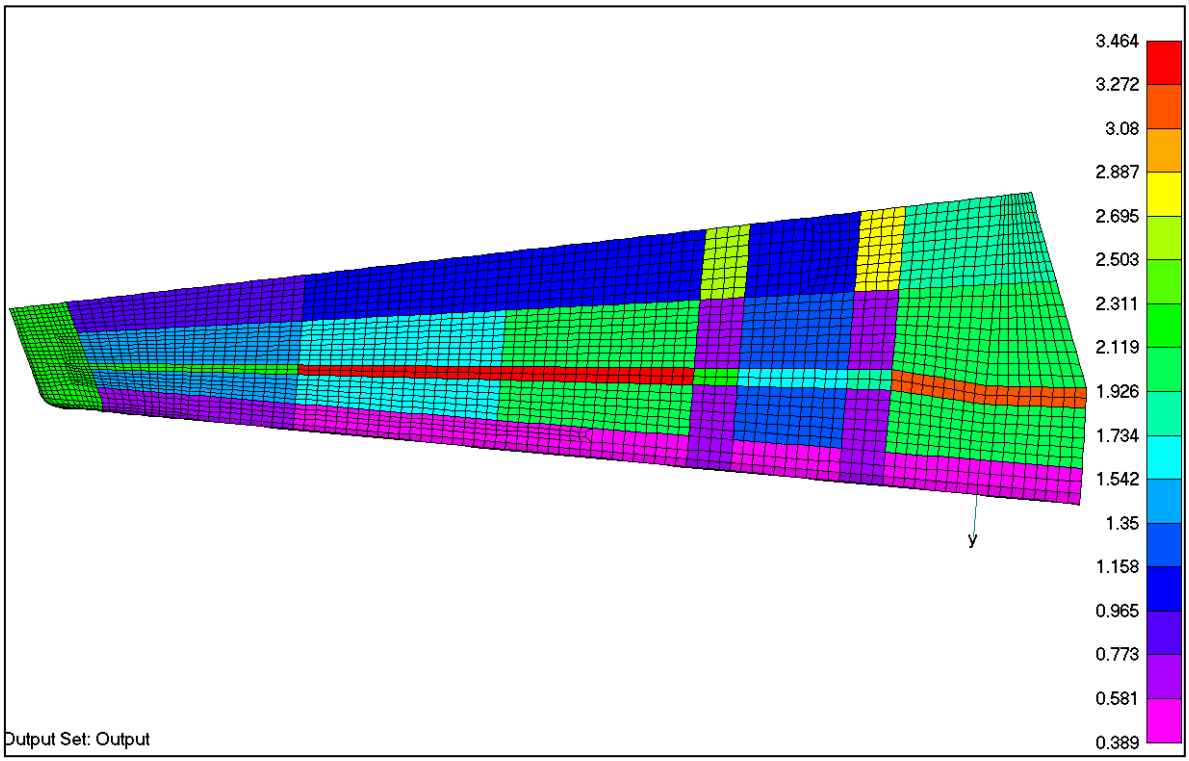

Figure 10 Rudder skin thickness for ΔT=-235

4. COMPARISON OF OPTIMAL DESIGNS

It is interesting to submit the optimal design obtained at a given optimization temperature to the three other distinct optimization temperatures. This is illustrated in Fig (11) where each curve corresponds to the stability behavior of an optimal design obtained for a given temperature.

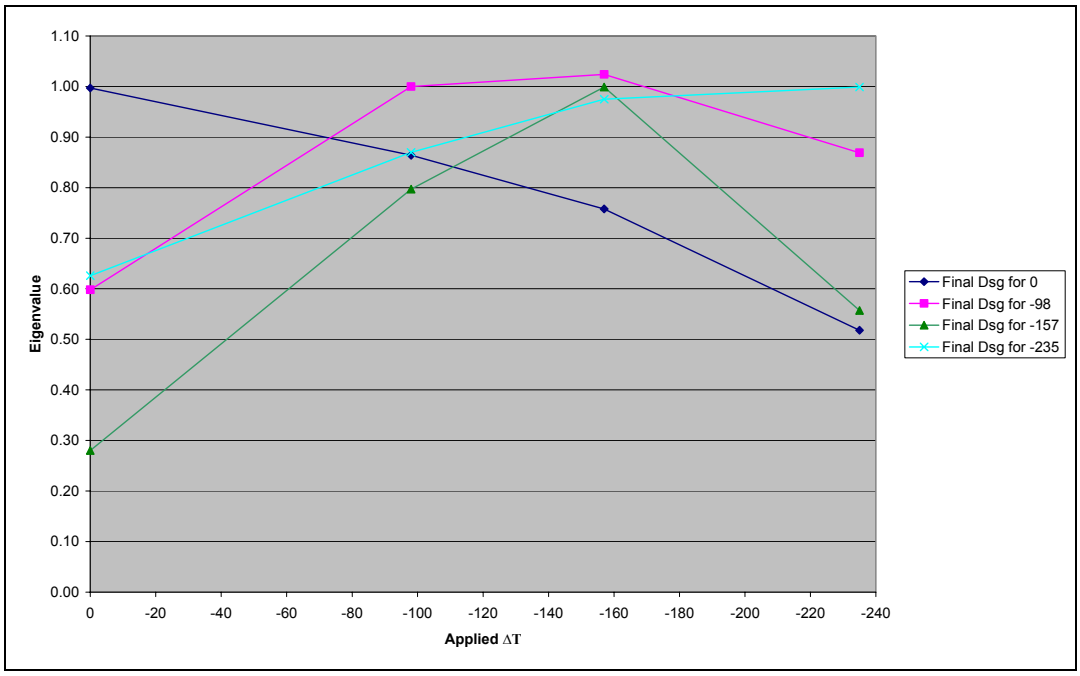

Figure 11 First eigenvalue evaluation for different optimized designs

From Fig. (11), it can be noticed that the maximum value of the fundamental eigenvalue occurs in each curve for the ΔT for which the rudder was optimized, except for the design at -98, where the temperature at -157 produces a slightly higher eigenvalue . This overall good behavior evidence that the optimization procedure herein described worked satisfactorily for the structure.

However it can be observed a significant decay of the fundamental eigenvalue for the rudder optimal designs in temperatures different from the one for which it was optimized. It is then apparent that the optimization of a structure taking advantage of thermal residual stresses should be made considering a service temperature range variation, since the curves on Fig. 11 present negative margins of safety for temperatures different from its own.

5. CONCLUSIONS

One can conclude that the optimization of complex composite laminated structures by applying TRS can be efficiently performed by MSC.NASTRAN but with caution and using the entire operational temperature envelope.

6. ACKNOWLEDGEMENTS

The first author acknowledges M.S. Riscado by its important contribution to this work providing the finite element mesh and support, and also Prof. Almeida for his inestimable advising.

7. REFERENCES

ALMEIDA, S. F. M.; HANSEN, J. S. Enhanced elastic buckling loads of composite plates with tailored thermal residual stresses. JOURNAL OF APPLIED MECHANICS, V. 64, p, 772-780, 1997

SARATH BABU, C.; KANT, T. Enhanced elastic buckling loads of composite plates with tailored thermal residual stresses. JOURNAL OF APPLIED MECHANICS, V. 65, n. 45, p, 1070-1071, 1998

ANDRADE, L. H. de, Otimização de Placas Laminadas com Tensões Residuais Térmicas em Problemas de Estabilidade Elástica e de Freqüências Naturais, INSTITUTO TECNOLÓGICO DE AERONÁUTICA, SÃO JOSÉ DOS CAMPOS, 2002, 211F

RISCADO, M.S. Projeto Estrutural e Definição de Processos de Fabricação de um Leme Aeronáutico em Material Compósito INSTITUTO TECNOLÓGICO DE AERONÁUTICA, SÃO JOSÉ DOS CAMPOS, 2004, 113F

8. RESPONSIBILITY NOTICE

The authors are the only responsible for the printed material included in this paper.